Isotope composition of secondary hydrogen and helium above the atmosphere measured by the instruments NINA and NINA-2

V. Bidoli,[1] M. Casolino,[1] M. De Pascale,[1] G. Furano,[1] A. Iannucci,[1] A. Morselli,[1] P. Picozza,[1] R. Sparvoli,[1] A. Bakaldin,[2] A. Galper,[2] S. Koldashov,[2] M. Korotkov,[2] A. Leonov,[2] V. Mikhailov,[2] S. Voronov,[2] M. Boezio,[3] V. Bonvicini,[3] A. Vacchi,[3] G. Zampa,[3] N. Zampa,[3] M. Ambriola,[4] F. Cafagna,[4] M. Circella,[4] C. De Marzo,[4] O. Adriani,[5] P. Papini,[5] P. Spillantini,[5] S. Straulino,[5] E. Vannuccini,[5] M. Ricci,[6] and G. Castellini[7]

Received 13 September 2002; revised 6 November 2002; accepted 5 February 2003; published 23 May 2003.

[1] In this paper we report on the energy spectra and abundance ratios of hydrogen and helium isotopes of albedo origin, measured by the instruments NINA and NINA-2 in near-equatorial regions. The instrument NINA flew on board the satellite Resurs-01-N4 between 1998 and 1999, at a 830 km average altitude. The NINA-2 apparatus, on board the satellite MITA, was put into orbit in July 2000 at an altitude of about 450 km. NINA and NINA-2 measurements revealed that ^{2}H, ^{3}H, ^{3}He, and ^{4}He are a significant portion of the secondary flux above the atmosphere. The energy spectra of hydrogen isotopes are practically flat across the energy range of 10–40 MeV/n, while the spectra of helium isotopes can be fitted by a power law of spectral indexes $\gamma = 0.8$ and $\gamma = 1.5$ for ^{3}He and ^{4}He, respectively. *INDEX TERMS:* 2479 Ionosphere: Solar radiation and cosmic ray effects; 2494 Ionosphere: Instruments and techniques; 2716 Magnetospheric Physics: Energetic particles, precipitating; 2720 Magnetospheric Physics: Energetic particles, trapped; *KEYWORDS:* isotopes, albedo, geomagnetic field, satellite, silicon detector

Citation: Bidoli, V., et al., Isotope composition of secondary hydrogen and helium above the atmosphere measured by the instruments NINA and NINA-2, *J. Geophys. Res.*, *108*(A5), 1211, doi:10.1029/2002JA009684, 2003.

1. Introduction

[2] The flux of high-energy particles produced by nuclear interactions of cosmic rays with residual atmosphere is composed mainly by electrons, positrons, protons, neutrons and gamma-rays, but also light nuclei are present. Secondary hydrogen and helium isotopes were observed by balloon experiments in different energy ranges [*Teegarden*, 1967; *Webber and Yushak*, 1983] and were studied as background component during measurements of primary cosmic ray nuclei [*Boezio et al.*, 2001; *Matsunaga et al.*, 1998]. The two main mechanisms that produce secondary light nuclei are air target nuclei break-up and fragmentation of incident nuclei. For energies lower than 100 MeV, the first reaction is dominant [*Vannuccini et al.*, 2001].

[3] An appreciable fraction of secondary particles, with rigidity less than the geomagnetic cut-off, can travel backward in space along the Earth's magnetic field and can be observed at satellite altitudes. Depending on their pitch angle, these particles oscillate in the geomagnetic field making only one bounce (so-called "reentrant albedo particles", absorbed in opposite hemisphere) or more than one bounce (quasi trapped albedo particles). There is also a fraction of albedo particles that can remain trapped for several years.

[4] As it was investigated by *Freden and White* [1960] this mechanism gives trapped light isotopes, but at least orders of magnitude less than interactions of trapped protons in the radiation belt with air nuclei. This second mechanism was later verified by detailed calculations done by *Selesnick and Mewaldt* [1996]. Their calculations are in good agreement with CRRES measurements of trapped He isotopes ratio [*Chen et al.*, 1996] and with measurements of trapped deuterium component done on board SAMPEX satellite [*Looper et al.*, 1996, 1998].

[5] On the other hand high-energy particles along unclosed drift trajectories may originate mainly from cosmic ray interactions with air nuclei. Recent measurements of the secondary light nuclear component above the atmos-

[1]Department of Physics, University of Rome "Tor Vergata" and Istituto Nazionale di Fisica Nucleare section of Roma2, Rome, Italy.
[2]Moscow Engineering Physics Institute, Moscow, Russia.
[3]Department of Physics, University of Trieste and Istituto Nazionale di Fisica Nucleare section of Trieste, Trieste, Italy.
[4]Department of Physics, University of Bari and Istituto Nazionale di Fisica Nucleare section of Bari, Bari, Italy.
[5]Department of Physics, University of Florence and Istituto Nazionale di Fisica Nucleare section of Florence, Florence, Italy.
[6]Istituto Nazionale di Fisica Nucleare National Laboratories of Frascati, Frascati, Italy.
[7]Institute of Applied Physics "Nello Carrara", CNR, Florence, Italy.

0148-0227/03/2002JA009684$09.00

phere were carried out on board the Space Shuttle by the AMS instrument [*Alcaraz et al.*, 2000]. Across the energy interval from 0.15 to several GeV/n, presence of ^{2}H and ^{3}He nuclei was detected. The tracing back of such particles in the geomagnetic field showed that they originate in atmosphere. Subsequent theoretical speculations, which investigated the behavior of primary and secondary particles in the geomagnetic field, confirmed the secondary origin of these particles [*Derome and Buenerd*, 2001; *Lipari*, 2002]. However, interaction of cosmic rays should produce also ^{3}H and ^{4}He whereas tritium was not observed by this experiment and only a lower limit on the ^{3}He/^{4}He ratio at E > 100 MeV/n was estimated (^{3}He/^{4}He $\geq$ 9).

[6] Moreover, no accurate measurements of the isotope composition of albedo and quasi trapped secondary light nuclei above the atmosphere below 100 MeV/n are available so far. This paper is focused on the measurements of the energy spectrum of light nuclei below the inner radiation belt, done by NINA and NINA-2 instruments between 10 and 40 MeV/n.

2. The NINA Experiments

[7] The satellite Resurs-01-N4 had a near-Earth polar orbit with inclination 98° and altitude of about 830 km. The mission NINA started on July 10th, 1998. The instrument was housed into Resurs on the top side external to the satellite, in such a way to point always to the zenith during the flight. The period of data taking lasted until April 1999; after this date, problems with the onboard transmitter stopped the data download.

[8] On 15 July 2000, a second detector, NINA-2, was placed in orbit housed into the Italian satellite MITA, in order to continue the scientific program of the NINA instrument extending its measurements in a different phase of the solar cycle. The satellite MITA was inserted into an almost circular polar orbit, with an inclination of about 87,3° and an altitude of about 450 km. Last data were taken on August 2001 at approximately 240 km of altitude, when the last radio contact was possible. The satellite had a three axes stabilization and measurements were carried out in two different modes: zenith orientation (axis of the instrument towards the zenith) and Sun orientation (axis of the instrument pointing to the Sun).

2.1. The Silicon Detector

[9] The NINA and NINA-2 instruments were based on the identical silicon detector, composed of 16 X-Y planes, each consisting of two n-type silicon elements, 60 × 60 mm^2, divided in 16 strips. The plane thickness is (2 × 150) μm for first plane, and (2 × 380) μm for the remaining 15 planes: the active part thus amounts to 11.7 mm.

[10] Interplanar distance is 1.4 cm for planes between 2 and 16 and 8.5 cm between plane 1 and 2 in order to improve the determination of the particle incident angle. The angular aperture of the telescope is about 32 degrees. The whole structure is surrounded by a cylindrical aluminum vessel 2 mm thick, except from a 300 μm thick window placed in front of the detector.

[11] The instrument has two different modes of particle detection: Low Threshold and High Threshold. In the first configuration the telescope can detect nuclei from hydrogen to iron across the full energy range (10–200 MeV/n), whereas in High Threshold mode it is possible to detect hydrogen isotopes only across a narrow range (11–16 MeV).

[12] The instrument performance was calculated by means of Monte Carlo simulations based on the CERN-GEANT 3.21 code [*Brun et al.*, 1994]. In addition, both detectors were calibrated at accelerator laboratories, with beam species from hydrogen to oxygen, across a wide energy interval. The geometric factor of the instrument ranges from 1 cm^{2}sr for particles crossing whole detector to 8.6 cm^{2}sr for low-energy particles. The mass resolution of the instrument is about 0.15 amu for He isotopes and about 0.1 amu for H isotopes. The energy resolution is better than 1 MeV. A detailed description of the instruments and their performance at beam facilities and in orbit are reported in the works by *Bidoli et al.* [1999, 2001] and *Casolino et al.* [2001].

2.2. Data Analysis

[13] The optimal performance of NINA in terms of charge, mass and energy determination is achieved by requiring the full containment of the particle inside the detector (up to ~40 MeV/n for hydrogen and helium isotopes). In addition, a dedicated off-line track selection algorithm is applied, which rejects upward moving particles, tracks accompanied by nuclear interactions, and events consisting of two or more tracks. In order to calculate the energy deposit (by means of the Bethe-Bloch formula) of the crossing particles in each layer of the detector, incident angles are taken into account. A detailed description of the selection algorithm can be found in the work of *Bidoli et al.* [2001].

[14] Charge and mass identification procedures are applied to events that survive the track selection algorithm. The mass M and the charge Z of the particles are calculated by the method of the residual range [*Cook et al.*, 1993; *Hasebe et al.*, 1993]. In this method, the charge Z is estimated by means of the product $E_1 \times E_{tot}$, and the mass is evaluated by applying the following formula:

$$M = \left(\frac{a\left(E_{tot}^{b} - (E_{tot} - \Delta E)^{b}\right)}{Z^2 \Delta x} \right)^{\frac{1}{b-1}}, \qquad (1)$$

where ΔE is the energy lost by the particle in a thickness Δx measured starting from the first plane. A precise evaluation of parameters a and b for each atomic species has been obtained both from beam test and simulated data [*Bidoli et al.*, 1999].

[15] The particle identification algorithm was previously tested with beam test data and used in the Galactic Cosmic Rays (GCR) analysis. It was found that it eliminates, together with the background, about 3% of tracks of real particles. A correction for this factor was introduced.

[16] As first step to determinate the energy of the detected particles, the sum of the energy deposits in the whole detector is calculated; energy losses in dead layers are then determined by interpolation formulas. Finally the incoming energy of the particles before the aluminum window is reconstructed by an iterative algorithm, based on the Bethe-Bloch formula using the known particle incident angle.

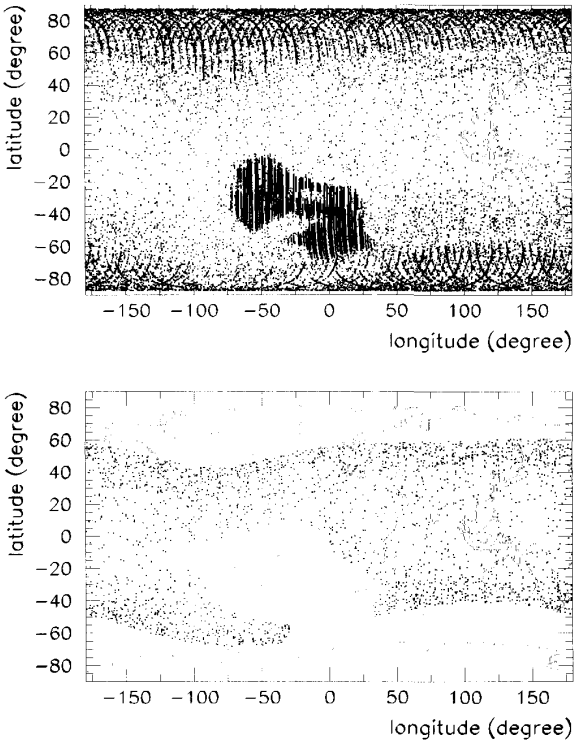

Figure 1. Top panel: map of events measured by NINA-2 in May and June 2001; bottom panel: events surviving after the selection criteria L-shell < 3 and B > 0.26 G.

[17] To evaluate the position of the satellite we use data from NORAD (see http://oig1.gsfc.nasa.gov/scripts/foxweb.exe/app01), while the geomagnetic coordinates L-shell and B are calculated by means of the IGRF (see http://nssdc.gsfc.nasa.gov/space/model/magnetos/igrf.html) model. To reconstruct the flux of a selected isotope, particles with mass out of two standard deviations from the correct isotope mass are rejected, compensating accordingly for the loss of good events.

[18] The particle differential energy spectra are determined by knowing the total counts, the exposure time in orbit for the period under consideration and the average value of the geometrical factor in each energy bin.

3. Results and Discussion

[19] Along their polar orbits, NINA and NINA-2 measured particles of galactic or solar origin, albedo particles coming from secondary production in atmosphere as well as particles trapped in the radiation belts. To separate the different families of particles, selections based on L-shell and B are used; in particular, our analysis has shown that a pure albedo component without contamination from trapped, galactic and solar particles, even during intense SEP events, is selected by L-shell < 3 and B > 0.26 G in NINA's energy range. At L-shell < 3, in fact, the geomagnetic cut-off is much higher than the particles rigidity in NINA's energy interval, so galactic protons of energy E < 100 MeV/n can reach neither Resurs nor MITA orbit. At small altitudes it is possible to observe trapped particles only inside South Atlantic Anomaly, where radiation belts are close to Earth's surface. Investigating the behaviour of fluxes as a function of B for MITA orbit at a fixed L-shell, it was found that the trapped population extends to B values up to 0.26 G (0.23 G for Resurs-01-N4); at higher values of B flux does not depend on B. The cut on B operates so to keep away the trapped component. It should be noted that, due to the orientation of the satellites, measured local pitch angles cover a range between 20° and 60° in the chosen region, with average value of about 45°. Such pitch angle values correspond to albedo particles, and that confirms the validity of our selection. In addition it is known that the geomagnetic cut-off can vary in case of intense SEP events, but during NINA and NINA-2 lifetimes none of these events changed appreciably the particle count rate at L-shell < 3.

[20] A sample of data measured in May and June 2001 before and after applying our selection criteria is shown in Figure 1. It is clear that the selection leaves only albedo particles. All data presented in the next figures refer to the restricted region L-shell < 3 and B > 0.26 G.

[21] Estimations of the secondary background for hydrogen and helium isotopes produced by cosmic rays inside the instrument, done with the method described by *Bakaldin et al.* [2002] that considers the first silicon detector as a target for secondary production, show that the contribution of this background in the count rate of nuclei is less than 8%.

[22] Figure 2 presents the mass reconstruction for particles with charge Z = 1 (left panel) and Z = 2 (right panel) detected by NINA-2. It is evident that NINA-2 detected the three hydrogen isotopes as well as ^{3}He and ^{4}He.

[23] Figure 3 presents the proton, deuterium and tritium fluxes, averaged in longitude, reconstructed by NINA-2. Results include data collected in both zenith and Sun orientation, as no statistically significant difference between the two orientations was found in NINA-2 proton analysis [*Bidoli et al.*, 2002]. In addition, no distinction has been made between albedo and quasi-trapped particles (i.e. between particles with different pitch angles). The hydrogen isotope fluxes in this energy region are rather flat.

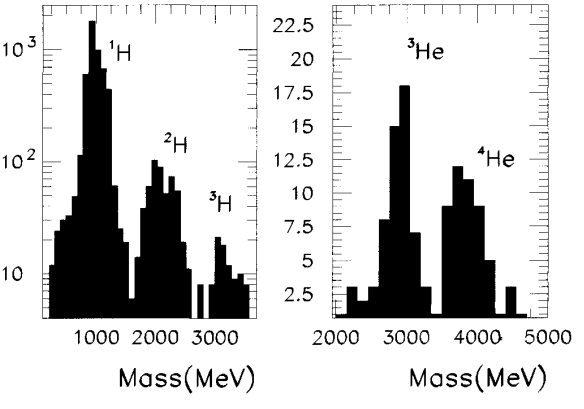

Figure 2. Mass distribution of particles with charge Z = 1 (left panel) and Z = 2 (right panel) at L-shell < 3 and B > 0.26 G, as measured by NINA-2.

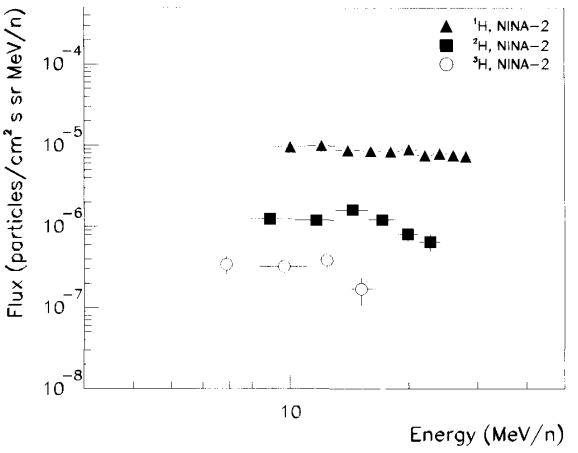

Figure 3. Differential energy spectra of secondary proton, deuterium and tritium at L-shell < 3 and B > 0.26 G, as measured by NINA-2.

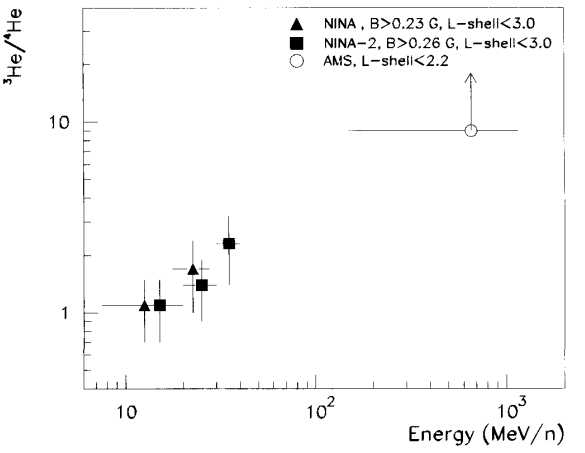

Figure 5. Albedo ^{3}He/^{4}He ratio, as measured by NINA and NINA-2. AMS lower limit for L-shell < 2.2 is also shown.

[24] Energy spectra of helium isotopes measured by NINA-2 instrument are presented in Figure 4, together with AMS results [*Alcaraz et al.*, 2000] and calculations done by *Derome and Buenerd* [2001]. Fitting NINA-2 data with the power law function $E^{-\gamma}$, the extracted spectral index is 0.8 ± 0.2 for ^{3}He and 1.5 ± 0.2 for ^{4}He.

[25] Helium isotope spectra in this energy region are evidently much steeper than proton ones. This is easily understood considering that the creation of the secondary flux takes place at an altitude of about 30–50 km [*Derome and Buenerd*, 2001; *Lipari*, 2002]. Before escaping from the atmosphere, secondary charged particles pass some quantity of material in air and lose energy. Differences in losses for hydrogen and helium due to their different charge explain the shape of their energy spectra.

[26] Figure 5 shows the ^{3}He/^{4}He ratio as a function of energy for NINA, NINA-2 and AMS; the agreement between NINA and NINA-2 data is good. The average value of the ^{3}He/^{4}He ratio across the energy range 10–40 MeV/n for both NINA experiments is ≃1.5. Data by NINA, NINA-2 and the lower limit by AMS show that the ^{3}He/^{4}He ratio increases from ≃1 to ≃9 across the energy range 10–1000 MeV/n. Similar results are observed for the helium trapped component in radiation belts [*Bakaldin et al.*, 2002], component originated by trapped proton interactions with residual atmosphere. As it was calculated by *Selesnick and Mewaldt* [1996], the ^{3}He/^{4}He ratio increases for trapped particles approximately in the same way as it does for albedo particles as seen by NINA.

[27] Figure 6 shows the ^{2}H/^{1}H, ^{3}H/^{1}H and ^{3}H/^{2}H NINA-2 abundance ratios as a function of energy. At low energy the

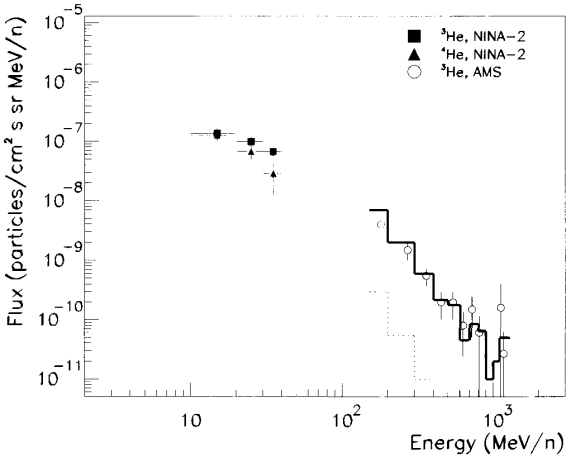

Figure 4. Secondary ^{3}He and ^{4}He flux as a function of energy, at L-shell < 3 and B > 0.26 G, as measured by NINA-2. Open points represents the sub-cutoff ^{3}He flux integrated over L-shell < 1.47, as measured by AMS [*Alcaraz et al.*, 2000]. Thick and dashed lines show simulation results corresponding respectively to the ^{3}He and ^{4}He flux [*Derome and Buenerd*, 2001].

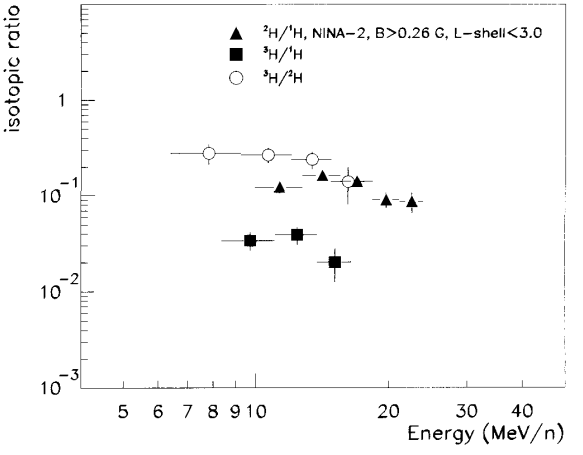

Figure 6. ^{2}H/^{1}H, ^{3}H/^{1}H, ^{3}H/^{2}H ratios at L-shell < 3 and B > 0.26 G, as measured by NINA-2.

$^2H/^1H$ ratio has a value of about 15% and decreases with increasing energy. This result is much higher than the $^2H/^1H$ ratio in the inner radiation belts measured by PET instrument on board SAMPEX [*Looper et al.*, 1996] and NINA instrument [*Bakaldin et al.*, 2002], which both observed a ratio of about 1%.

[28] At energy of about 150 MeV/n, $^2H/^1H$ ratio of albedo particles is between 2% and 5%, as measured by AMS [*Lamanna et al.*, 2001]. It is known that ^2H isotope is very rare in nature, typically with a concentration lower than 10^{-5} [*Mullan and Linsky*, 1998]. Albedo deuterium is probably the highest concentration of deuterium existing in nature.

[29] As for tritium, NINA-2 measured a $^3H/^2H$ ratio of about 0.25 and a $^3H/^3He$ ratio of about 3 at $\simeq$10 MeV/n. NINA and NINA-2, differently from the recent measurements by AMS, detected an appreciable quantity of albedo tritium. As said in the introduction, air target nuclei break-up is the most probable process to explain light isotope abundances at low energy. Such reactions produce also tritium. The quasi deuteron nuclei model suggests that the $^2H/^3H$ ratio increases with energy, for energies greater than 30 MeV/n, and that can be the reason why AMS did not detect tritium at high energy. Data from accelerators experiments seem to confirm this assumption. For example, it was measured by *Wu et al.* [1979] that for a 90 MeV proton projectile on ^{27}Al, ^{58}Ni, ^{90}Zr, ^{209}Bi the average ratio $^2H/^3H$ was about 5, in agreement with NINA measurements. At the same time, a calculation at energy more 150 MeV/n done by *Derome and Buenerd* [2001] gives a $^2H/^3H$ ratio between 20 and 50.

4. Conclusions

[30] NINA and NINA-2 detectors have verified the existence of fluxes of light isotopes below the geomagnetic cutoff. NINA flew on board Resurs-01-N4 satellite in a 830 km average altitude orbit between 1998 and 1999 and NINA-2 flew on board the MITA satellite at an altitude of about 450 km in 2000–2001.

[31] The good mass resolution of NINA and NINA-2 detectors allowed distinguishing hydrogen and helium isotopes, including ^3H and ^4He which had been not observed in albedo fluxes above the atmosphere before.

[32] NINA and NINA-2 measured the $^2H/^1H$ ($\simeq$15%), $^3H/^2H$ ($\simeq$25%), $^3H/^1H$ ($\simeq$4%), $^3H/^3He$ ($\simeq$3) and $^3He/^4He$ ($\simeq$1.5) isotope abundance ratios, and reconstructed the differential energy spectra of all hydrogen and helium isotopes of albedo origin across the energy interval 10–40 MeV/n.

[33] **Acknowledgments.** Shadia Rifai Habbal thanks Richard Selesnick and J. Bernard Blake for their assistance in evaluating this paper.

References

Alcaraz, J., et al., Helium in near Earth orbit, *Phys. Lett. B*, *494*, 193–202, 2000.

Bakaldin, A., et al., Geomagnetically trapped light isotopes observed with the detector NINA, *J. Geophys. Res.*, *107*(A8), 1171, doi:10.1029/2001JA900172, 2002.

Bidoli, V., et al., The space telescope NINA: Results of a beam test calibration, *Nucl. Instrum. Methods Phys. Res., Sect. A*, *424*, 414–424, 1999.

Bidoli, V., et al., In-orbit performances of the space telescope NINA and GCR fluxes measurements, *Astrophys. J. Suppl. Ser.*, *132*, 365–375, 2001.

Bidoli, V., et al., Energy spectrum of secondary protons above the atmosphere measured by the instruments NINA and NINA-2, *Ann. Geophys.*, *20*, 1693–1697, 2002.

Boezio, M., et al., The cosmic-ray antiproton flux between 3 and 49 GeV, *Astrophys. J.*, *561*, 787–799, 2001.

Brun, R., et al., Detector description and simulation tool, *CERN Program Libr.*, Eur. Org. for Nucl. Res., Geneva, 1994.

Casolino, M., et al., Launch in orbit of the NINA-2 apparatus aboard the satellite MITA, *Proc. 27 ICRC (Hamburg)*, *6*, 2314–2317, 2001.

Chen, J., et al., Energetic helium isotopes trapped in the magnetosphere, *J. Geophys. Res.*, *101*, 24,787–24,799, 1996.

Cook, W. R., et al., MAST: A Mass Spectrometer Telescope for studies of the isotopic composition of solar, anomalous and galactic cosmic ray nuclei, *IEEE Trans. Geosci. Remote Sens.*, *31-3*, 557–564, 1993.

Derome, L., and M. Buenerd, Origin of light nuclei in near Earth orbit, *Phys. Lett., B*, *521*, 139–145, 2001.

Freden, S. C., and R. S. White, Particles fluxes in the inner radiation belt, *J. Geophys. Res.*, *65*, 1377–1383, 1960.

Hasebe, N., et al., Improvement of mass resolution of cosmic ray nuclei using a $\Delta E \times \Delta E$ Si detector telescope, *Nucl. Instrum. Methods Phys. Res. A*, *325*, 335–342, 1993.

Lamanna, G., et al., Measurement of deuteron spectra in Low Earth Orbit with the Alpha Magnetic Spectrometer, *Proc. 27 ICRC (Hamburg)*, *5*, 1614–1617, 2001.

Lipari, P., The fluxes of sub-cutoff particles detected by AMS, the cosmic ray albedo and atmospheric neutrinos, *Astroparticle Phys.*, *16*, 295–323, 2002.

Looper, M. D., et al., SAMPEX observations of energetic hydrogen isotopes in the inner zone, *Radiat. Meas.*, *26*, 967, 1996.

Looper, M. D., et al., Maps of hydrogen isotopes at low altitudes in the inner zone from SAMPEX observations, *Adv. Space Res.*, *21*, 1679, 1998.

Matsunaga, H., et al., Measurement of low-energy cosmic-ray antiprotons at solar minimum, *Phys. Rev. Lett.*, *81*, 4052–4055, 1998.

Mullan, D. J., and J. L. Linsky, Nonprimordial deuterium in the interstellar medium, *Astrophys. J.*, *511*, 502–512, 1998.

Selesnick, R. S., and R. A. Mewaldt, Atmospheric production of radiation belt light isotopes, *J. Geophys. Res.*, *101*, 19,745–19,757, 1996.

Teegarden, B. J., Cosmic-ray production of deuterium and tritium in the Earth atmosphere, *J. Geophys. Res.*, *72*, 4863–4868, 1967.

Vannuccini, E., C. Grimani, P. Papini, and S. A. Stephens, An estimate of the secondary ^2H spectrum produced by cosmic rays in the atmosphere, *Proc. 27 ICRC (Hamburg)*, *5*, 4181–4184, 2001.

Webber, W. R., and S. M. Yushak, A measurement of the energy spectra and relative abundance of the cosmic-ray H and He isotopes over a broad energy range, *Astrophys. J.*, *275*, 391–404, 1983.

Wu, J. R., C. C. Change, and H. D. Holmgren, Charged-particle spectra: 90 MeV protons on ^{27}Al, ^{58}Ni, ^{90}Zr, ^{209}Bi, *Phys. Rev., C*, *19*, 698–713, 1979.

O. Adriani, P. Papini, P. Spillantini, S. Straulino, and E. Vannuccini, Department of Physics, University of Florence and Istituto Nazionale di Fisica Nucleare section of Florence, Largo Enrico Fermi 2, I-50125 Florence, Italy.

M. Ambriola, F. Cafagna, M. Circella, and C. De Marzo, Department of Physics, University of Bari and Istituto Nazionale di Fisica Nucleare section of Bari, Via Amendola 173, I-70126 Bari, Italy.

A. Bakaldin, A. Galper, S. Koldashov, M. Korotkov, A. Leonov, V. Mikhailov, and S. Voronov, Moscow Engineering Physics Institute, 115409 Moscow, Russia.

V. Bidoli, M. Casolino, M. De Pascale, G. Furano, A. Iannucci, A. Morselli, P. Picozza, and R. Sparvoli, Department of Physics, University of Rome "Tor Vergata" and Istituto Nazionale di Fisica Nucleare - Via della Ricerca Scientifica 1, 00133 Rome, Italy. (alessandro.iannucci@roma2.infn.it; Roberta.Sparvoli@roma2.infn.it)

M. Boezio, V. Bonvicini, A. Vacchi, G. Zampa, and N. Zampa, Department of Physics, University of Trieste and Istituto Nazionale di Fisica Nucleare section of Trieste, Via A. Valerio 2, I-34147 Trieste, Italy.

G. Castellini, Institute of Applied Physics "Nello Carrara", CNR, Via Panciatichi 64, I-50127 Florence, Italy.

M. Ricci, Istituto Nazionale di Fisica Nucleare National Laboratories of Frascati, Via Enrico Fermi 40, I-00044 Frascati, Italy.